Enhancing colloid stability of polymer microspheres in water through SiO_2 coating
Effects of coating cycles and surface coverage

Kamphorst, Rens; Wanjari, Pratyush; Saedy, Saeed; van Dam, Julia F.K.; Thijssen, Arjan; Brüner, Philipp; Grehl, Thomas; Meesters, Gabrie M.H.; van Ommen, J. Ruud

DOI
10.1016/j.surfin.2024.103852

Publication date
2024

Document Version
Final published version

Published in
Surfaces and Interfaces

Surfaces and Interfaces 45 (2024) 103852

Contents lists available at ScienceDirect

Surfaces and Interfaces

journal homepage: www.sciencedirect.com/journal/surfaces-and-interfaces

Enhancing colloid stability of polymer microspheres in water through SiO_2 coating: Effects of coating cycles and surface coverage

Rens Kamphorst [a,*], Pratyush Wanjari [a], Saeed Saedy [a], Julia F.K. van Dam [a], Arjan Thijssen [a], Philipp Brüner [b], Thomas Grehl [b], Gabrie M.H. Meesters [a], J. Ruud van Ommen [a,*]

[a] Department of Chemical Engineering, Delft University of Technology, Delft, The Netherlands
[b] ION-TOF GmbH, Münster, Germany

ARTICLE INFO

Keywords:
Surface functionalization
Atomic layer deposition
Chemical vapor deposition
Wettability
Agglomeration

ABSTRACT

In this study, we investigated the wettability and agglomeration characteristics of polymer microspheres coated with low-temperature deposited SiO_2 in a fluidized bed atomic layer deposition (ALD) setup. Surface characterization revealed the presence of a significant amount of deposited Si-OH groups within the first cycles. A drastic decrease in agglomerate size, water contact angle (WCA), and droplet absorption time of the powder was observed when coating was applied. Furthermore, we observed an increase in the amount of Si-OH present on the particle surface with increasing coating cycles, while no significant improvement in water affinity was found after the first coating cycles. Our findings suggest that surface coverage is the primary factor in improving the colloid stability of particles, coated at low temperatures. The low temperature operation of our system introduced a chemical vapor deposition (CVD) component to our coating process, which allowed full surface coverage to be achieved within the first two coating cycles.

1. Introduction

Fine particles dispersed in a liquid medium have extensive applications in various fields, examples of which are food [1,2], drug-delivery [3], composites [4], and paints [5]. Due to their small size, the gravitational force acting on these particles is negligible, the stability of a colloidal suspension containing such particles is predominantly determined by the affinity of the solid surface groups with the liquid medium [6]. In the absence of adequate repulsion forces, van der Waals forces are dominant, causing particle clustering and eventual growth to a size where buoyancy induces phase segregation.

Since the affinity of the solid particles with the liquid medium is a surface characteristic, manipulating the surface groups is an effective lever to control the stability of liquid–solid dispersions. Various coating techniques have demonstrated their potential to stabilize the solid–liquid mixture without the need for a surfactant [7]. Of these techniques, atomic layer deposition (ALD) is an attractive option since it can deposit conformal, ultra-thin films, preserving the bulk properties of the coated substrate [8]. In this coating process, one or more precursor(s) and oxidizer(s) are introduced sequentially, with a purge step in between. The reactants are carefully chosen, such that they react in a self-limiting way with the substrate surface, depositing no more than one monolayer per coating cycle [9]. Coating thickness is controlled by selecting the amount of cycles. To obtain complete self-limiting behavior, the coating should take place within the ALD temperature window, which is typically at elevated temperatures. This limits the applicability and precursor options of the ALD process when dealing with temperature-sensitive substrates.

ALD is often seen as a specific type of chemical vapor deposition (CVD) [10]. In standard CVD, the precursor and oxidizer are typically introduced simultaneously. In the absence of a purge step, the reactants tend to physisorb onto the substrate surface and directly react with on another. This typically results in faster deposition and thicker coatings compared to ALD. Coating thickness is controlled by reaction time. CVD has the benefit of faster growth rates, but provides limited coating uniformity [11].

The application of such coating techniques on flat substrates is relatively straightforward. When dealing with particles however, a fluidized bed is often employed [12,13]. Here, the powder is present in a column and gas in introduced from the bottom, creating drag and lifting up the particles, provided the system is operated above the so called minimum fluidization velocity. When in the fluidized state, gas–solid contact is maximized, allowing for efficient coating deposition on the particles. Due to the cohesive nature of small particles, fluidization becomes troublesome as slugging, channeling and excessive agglomeration can occur [14,15], all of which limit gas–solid interactions. To overcome these issues, assistance methods, like

* Corresponding authors.
E-mail addresses: R.kamphorst@tudelft.nl (R. Kamphorst), J.R.vanOmmen@tudelft.nl (J.R.v. Ommen).

https://doi.org/10.1016/j.surfin.2024.103852
Received 27 October 2023; Received in revised form 11 December 2023; Accepted 3 January 2024
Available online 6 January 2024

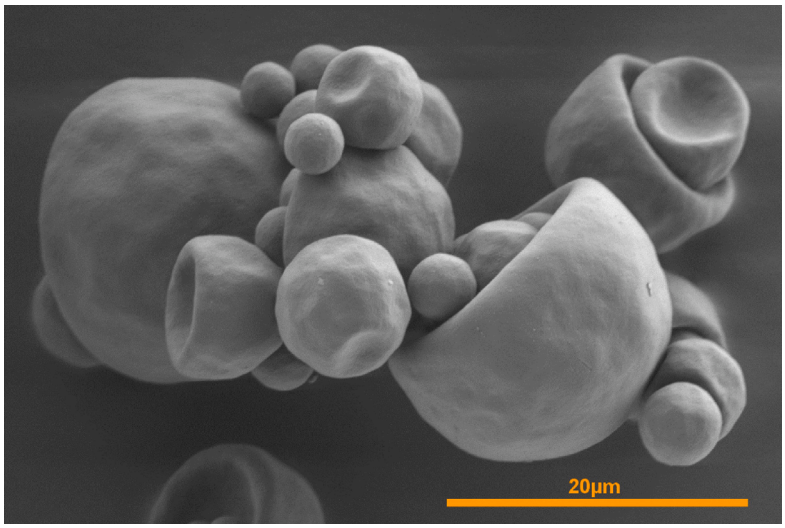

Fig. 1. SEM image of Expancel® polymer microspheres.

mechanical vibration [16,17] and pulsed flow operation [18], can be introduced, which can break pre-existing structures and maintain a well-mixed emulsion phase.

In the present study, we improved the wettability of temperature sensitive polymer microspheres by depositing an SiO_2 coating, employing an fluidized bed ALD setup. The temperature sensitive substrate we aim to modify, necessitates operating at low temperatures. Consequently, not all reactants adsorbed on the substrate surface will be removed during the purge steps, resulting in CVD behavior, drastically increasing the deposition per coating cycle. We expect this to result in faster complete surface coverage, which we anticipate to be beneficial for this particular application. By operating in a pulsed, ALD-like, manner, we maintain control over the amount of deposition on the polymer particles. We demonstrate complete surface coverage was obtained within the first two deposition cycles. Furthermore, it is shown that the introduction of functional surface groups improved wettability and colloid stability. Our results provide insight into the dominant parameters of improved colloid stability by surface modification when applying coatings on temperature-sensitive substrates.

2. Methods and materials

2.1. Substrate

For this study, Expancel® polymer micro-spheres (provided by Nouryon) were used. An SEM image of the Expancel particles is show in Fig. 1. These particles are a methylmethacrylate–acrylonitrile co-polymer, which has a glass transition temperature of 90 °C, necessitating low temperature operation when depositing functional surface groups. The polymer shell encloses a driving gas, making that heating this powder to temperatures beyond 90 °C induces swelling of the particles, resulting in a volume increase of up to 60 times the initial volume. This property makes for a versatile product, which is, among other applications, used in paint, shoe soles, artificial leather, and printing ink. In Fig. 2 the volume-based particle size distribution, as determined by a Malvern3000 particle size analyser, is shown.

2.2. Deposition setup

The particles were coated in a fluidized bed ALD setup, utilizing $SiCl_4$ and H_2O as reactants. A vibrating table was employed, operated at a frequency of 50 Hz and 0.015 mm amplitude to mitigate channel formation of the cohesive powder. Furthermore, since this powder proved to be exceptionally cohesive, we sieved with a 600 µm mesh size to remove pre-existing agglomerates and increase aeration of the bulk powder prior to fluidization. A glass column, with an inner diameter of 2.5 cm equipped with a heating jacket to maintain a constant temperature of 50 °C, as measured in the core of the reactor column, was used. The precursor bubblers were not heated (the ambient temperature was 25 °C), while the outlet lines of the bubblers and makeup stream line were heated to 30 °C, as was the windbox. Pulse times of 30 s for $SiCl_4$ and 45 s for H_2O were used with dry nitrogen as carrying gas; a N_2 purge time of 5 min was maintained between pulse steps. Additionally, a N_2 makeup stream was employed to maintain an equal gas flow during pulse and purge steps, assuring stable fluidization at constant a superficial gas velocity of 17 cm s^{-1}. During pulse steps, the ratio of pulse to makeup stream was 1:10. After every pulse step, the gas flow was interrupted for 15 s to allow for a back-pulse, preventing clogging of the top distributor plate, after which the fluidization was initiated again. After the final pulse step, the bed was purged for an additional 10 min before terminating the experiment. About 5 g of powder was coated during each experiment.

2.3. Characterization

Fourier Transform Infrared Spectrometry Attenuated Total Reflection (FTIR-ATR) was employed to identify surface groups on both coated and uncoated samples using the Nicolet 6700 spectrometer by ThemoFischer.

Additionally, the surface chemistry of uncoated and coated substrates was studied using X-ray photoelectron spectroscopy (XPS). For this purpose, a Thermo Scientific K-Alpha spectrometer, utilizing a monochromatic aluminum Kα radiation with a photon energy of 1486.7 eV, was used. An elliptical X-ray spot of 700 × 400 µm^2 was radiated to the surface of the samples, and the differential charging was compensated using a flood gun. Using such a large probe size, compared to the individual Expancel® particle size, results in proper signal quality, statistically representing the average of the samples. The pristine and as-coated samples were stabilized on the sample holder using conductive carbon tape and transferred into the measurement chamber of the machine. The survey scans with a resolution of 1.0 eV were acquired to have an overall view of the surface chemistry of the sample and high-resolution spectra of the elements of interest (C, O, N, Si, and Cl) with a resolution of 0.1 eV. The obtained XPS spectra were analyzed using CasaXPS software. The peak positions were calibrated with reference to the aliphatic carbon 1s peak (284.8 eV). The chemical composition of the surface of investigated samples was quantified by taking into account the peak area (peak integration) of the studied

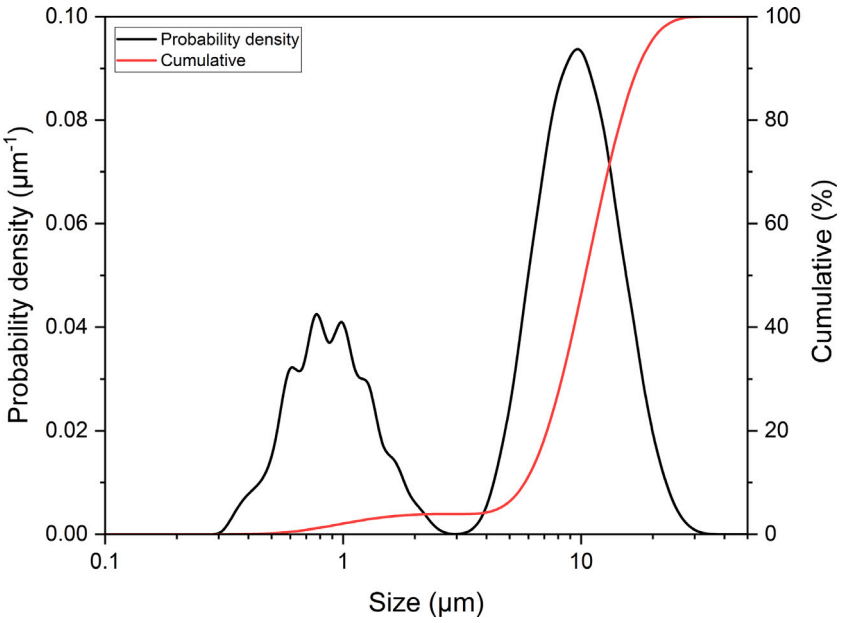

Fig. 2. Volume-based particle size distribution of Expancel® polymer microspheres.

elements after defining the quantification regions for each element, in CasaXPS.

To assess the surface coverage attained after coating we employed Low Energy Ion Scattering (LEIS). This technique offers the unique quality of having virtually no penetration depth, the measured signal originating the very top layer of a substrate surface [19]. This allows to establish whether full surface coverage is achieved, even if by a very thin layer of deposited material, from disappearance of substrate related peaks. The experiments were carried out using a Double Toroidal Energy Analyser by IONTOF, which used Helium ions and operated at an incident ion energy of 3000 eV, scattering angle of 145°.

Environmental Scanning Electron Microscopy (ESEM) was utilized to image the particles in the presence of moisture. To this end, a FEI Quanta FEG 650 was employed utilizing a peltier cooling stage, operated at 0.5 °C, and operating pressures between 6–8 mbar to obtain water condensation.

Focused Beam Reflectance Measurements (FBRM) were performed for in-situ agglomerate size measurements, using the FBRM G400 by Mettler Toledo. The measured cord lengths were converted to diameters, using the ratio between the average cord length of a circle to its diameter. The powder sample was suspended in ultra-pure (Milli-Q) water at a loading of 20 g L^{-1}. For each experiment, the mixture was sonicated for 10 min prior to measuring the cluster size. Measurements were performed at room temperature, and a magnetic stirrer, rotating at 100 rpm, was employed during the entire runtime of the experiment. Data points were collected every 10 s; experiments lasted for a total of 60 min.

The water contact angle (WCA) was measured using the Drop Shape Analysis System by Kruss Scientific GmbH. To obtain a flat surface, (coated) powder was compressed into 1.0 cm diameter tablets by applying 1.0 tonne of pressure for 15 s, and droplets of 5 μL were placed onto the tablets at room temperature. The angle was measured immediately after the water–tablet contact. In addition, the duration of droplet infiltration into the tablet pores was recorded to yield supplementary insights on the affinity between the water and the substrate.

3. Results and discussion

3.1. Surface characterization

The particles were subjected to FTIR-ATR to investigate the presence of Si surface species on coated substrates. To demonstrate the presence of SiO_2 after deposition, an isolated signal, originating from the applied coating, obtained by subtracting the signal from the uncoated sample from the coated one (10C raw), resulting in a differential signal (10C differential), is displayed in Fig. 3. The highlighted regions of interest indicate the formation of Si-related groups and suppression of substrate-related peaks. The inverse peak observed in the differential signal in region **A** is caused by attenuation of the C=O response by the coating layer formed on top of the pristine sample. This region offers insights into film growth, as displayed in Fig. 4. Note that the absorbance is plotted on the *y*-axis. We de-convoluted the raw signal by peak-fitting to determine the area of the C=O peak in each sample respectively (note the slight peak at 1630 cm^{-1} and the right shoulder to the C=O peak for the pristine sample). This area, normalized to the area peak of uncoated powder is shown in the inset. The coating layer reduced the peak intensity by each additional cycle. The inset in Fig. 4 depicts a steep decrease in peak area upon the first cycle, with additional attenuation upon further deposition. Furthermore, the inset displays a considerably higher decrease in peak area upon the first coating cycle, compared to the near linear decrease found for consecutive cycles.

In Fig. 5, we present the FTIR-ATR spectra within the region where Si-related peaks occur. It can be observed that the peak heights found at 930 cm^{-1} and 1070 cm^{-1} grow with increasing deposition cycles. The 930 cm^{-1} peak is attributed to Si–OH bending [20–22] and the 1070 cm^{-1} peak corresponds to asymmetric Si–O–Si stretching [23]. Furthermore, for 5 and 10 cycles of deposition, an additional peak becomes visible at 800 cm^{-1}, which corresponds to symmetric stretching Si–O–Si [23]. This peak is partially obscured at lower amount of cycles due to the substrate peaks at 760 cm^{-1} and 850 cm^{-1}. These peaks, as well as the one at 980 cm^{-1} again show signal suppression of the substrate when the amount of coating cycles is increased. The inset in Fig. 5 provides insight into the relative growth rate of Si–O–Si and Si–OH groups (normalized to the area underneath the C=O peak of the pristine sample, for Si–O–Si only the area of the peak corresponding to asymmetric stretching is considered). Since Si–OH groups are anticipated to be present mostly on the surface of the sample, and are expected to be consumed in the precursor step by forming O–Si–Cl bonds, the observed lower relative value is expected. The continuous growth of this peak during the first 10 cycles indicates coating deficiencies, where not all Si–OH groups react upon the introduction of $SiCl_4$ during the precursor step and some are built into the coating. The inset also shows

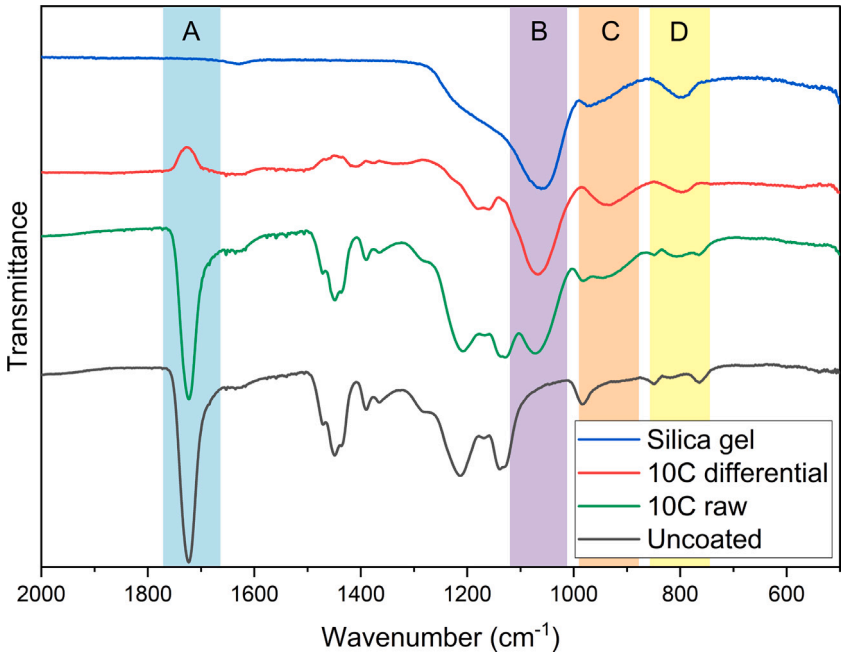

Fig. 3. FTIR-ATR spectrum overview, **A** : C=O stretch, **B** : asymmetric Si–O–Si stretch, **C** : Si–OH bend, **D** : symmetric Si–O–Si.

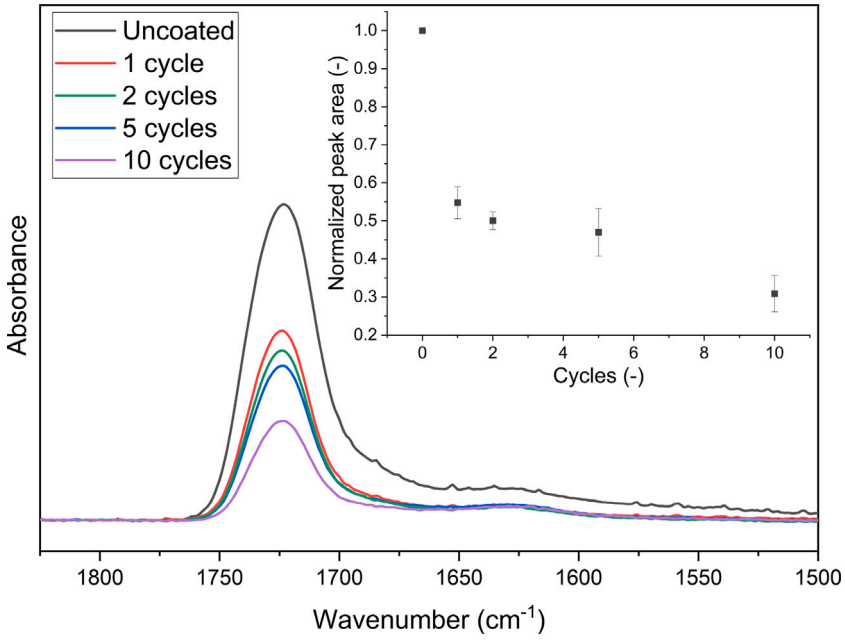

Fig. 4. FTIR-ATR spectra showing decreasing intensity of C=O peak, due to signal attenuation when increasing the amount of coating cycles. In the inset normalized C=O peak areas after various amounts of deposition cycles are displayed.

a pronounced initial slope for both Si-groups, followed by a, less steep, linear growth upon additional deposition cycles.

The XPS experimental results are presented in Fig. 6. First of all, it is evident that the coating incorporates negligible amounts of chlorine. This finding indicates that the oxidizer step of the coating cycles reaches full completion. However, considering the results presented in Fig. 5, the precursor step does not reach completion, as the amount of Si–OH groups keeps increasing with additional coating cycles. Additionally, the atomic percentage of Si and O demonstrates an initial increase in the first coating cycle, followed by a stable composition in subsequent deposition cycles. This observation leads us to conclude that a coating layer thicker than the XPS signal's penetration depth (approximately 4 nm) is deposited during the first coating cycle. This outcome aligns with the FTIR-ATR data, although the greater penetration depth of that technique allows for subsurface information to be obtained, even after multiple coating cycles. Finally, the presence of carbon (note the double *y*-axis) originates from incidental groups formed due to sample exposure to the atmosphere.

LEIS experiments were performed to assess the surface coverage of coated samples, the results of which are displayed in Fig. 7. Here it is demonstrated that the spectra of the coated particles did not change with an increasing number of coating cycles; note that we tested a sample coated with 100 cycles to assure of no changes upon excessive additional deposition. Furthermore, in contrast to the signal obtained by XPS, the carbon related signal found by LEIS is absent after a single coating cycle already. Additionally, the absence of a

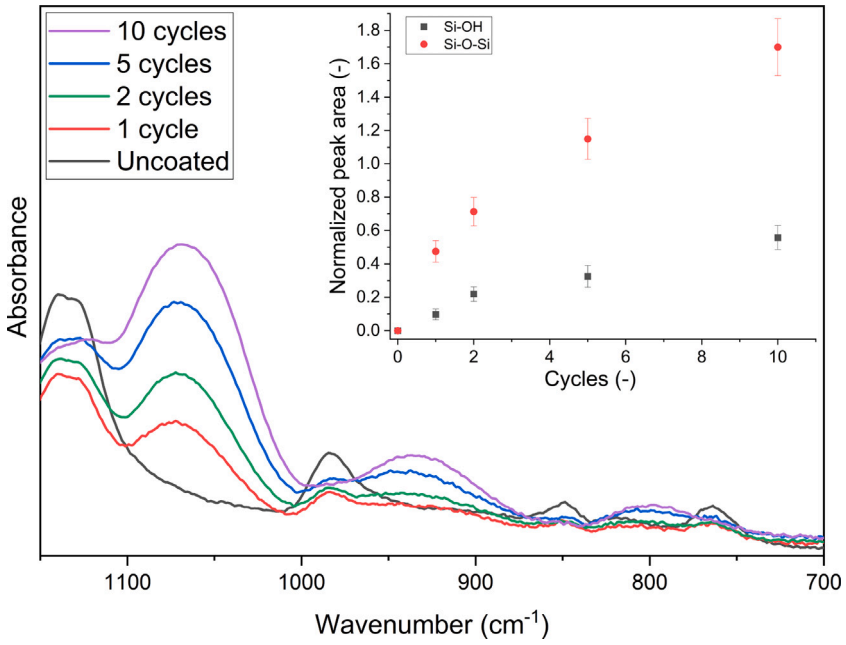

Fig. 5. FTIR-ATR spectra showing growth of Si-related peaks when increasing the amount of coating cycles. In the inset normalized areas of O–Si–O and Si–OH peaks after various amounts of deposition cycles are displayed.

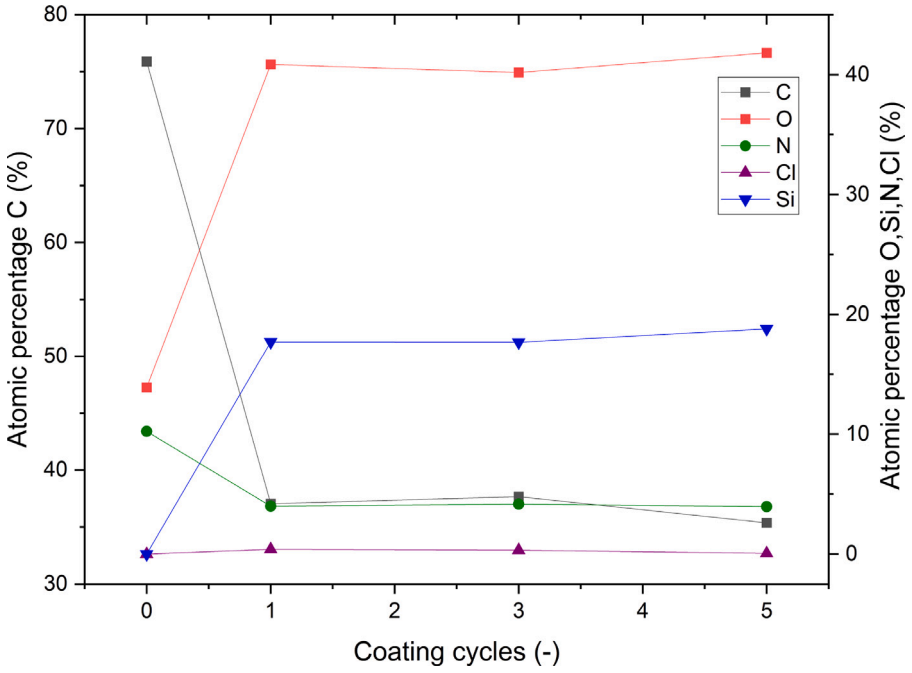

Fig. 6. Atomic percentage of elements found on the particle surface, obtained via XPS.

chlorine peak, which would appear at 1950 eV if present, re-affirms completion of the oxidizer step of the coating process. Our findings indicate that full surface coverage was achieved after a single coating cycle. Furthermore, the non-zero signal between the O and Si peaks originates from subsurface Si. Note that this is observed after 1 coating cycle and is not changing with additional deposition. This confirms the conclusions drawn earlier from the XPS data that more than a mono-layer of coating is deposited after in the first coating cycle. From additional experiments utilizing focused ion beam SEM, it was found that the coating thickness of all samples in this study was well below 80 nm, though an exact thickness could not be obtained, see the supplementary materials for more details.

Based on the analysis of FTIR-ATR, XPS, and LEIS results, we expect the presence of adsorbed moisture on the particle surface during the initial coating cycle, which could not entirely be removed due to the low temperature operation. Adsorption of ultra-thin layers of moisture is known to occur on hydrophilic, and even to some extent on hydrophobic particles [24]. When present, this moisture contributes to the formation of a comparatively thick and conformal coating during the first deposition cycle, which subsequently increases in thickness with additional coating cycles. This observation provides a plausible explanation for several findings. Firstly, LEIS analysis indicates complete surface coverage following the first cycle. Secondly, XPS analysis confirms a substantial deposition thickness after the initial cycle. Lastly,

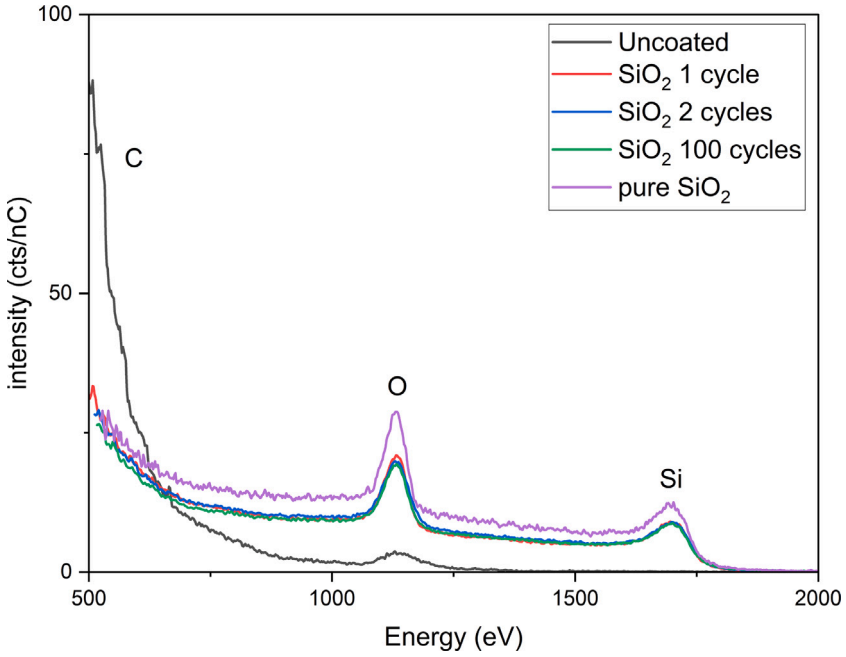

Fig. 7. LEIS results of pristine sample, coated samples and SiO_2 powder.

FTIR-ATR data reveals a higher deposition amount in the first cycle compared to subsequent cycles. These observations collectively highlight key distinctions between the conventional ALD coating process and the pulsed CVD coating process employed in our study.

3.2. Wettability and agglomeration

In order to provide a qualitative evaluation of the improved wettability of the coated particles, we utilized ESEM to visualize the particles in the presence of moisture. The image of uncoated particles, Fig. 8, demonstrates limited affinity with water, as the surface of the particles appear completely devoid of moisture. In contrast, the coated particles, seen in Figs. 9 to 11 display a marked affinity with water. The imaged agglomerates tended to absorb water to a high extent, resulting in their entire surface being covered by water. Furthermore, individual particles were observed to adsorb water, and form a layer of water onto their surfaces too. Based on these images, it is evident that there is a discernible distinction in behavior between the coated and uncoated particles when brought in contact with water. It should be noted that the clustering of the coated particles observed in the images is a result of the coating process, in which agglomerates are formed in the fluidized bed. All of the agglomerates imaged in this study were present prior to the introduction of moisture in the ESEM.

To gain further insight into the phenomenon observed in the ESEM images, and to allow the results to be quantified, we also considered the results of the FBRM. Fig. 12 illustrates the development of the agglomerate size distribution in water of the experiment where uncoated particles are studied. Note that the vast majority of primary particles of the pristine powder were found to have a size below 20 µm (Fig. 2). Therefore, only the measured entities with a diameter above 20 µm can reliably be identified as agglomerates. It was observed that the agglomerates initially grow upon contact with water, which is highlighted in the inset of Fig. 12. This behavior re-establishes the limited affinity of the pristine powder with water. In contrast, particles coated with SiO_2 for only 1 cycle show no significant change in agglomerate size formation over time, when brought in contact with water, as can be observed in Fig. 13. Furthermore, when 2 coating cycles are deposited, the agglomerate size even decreases initially before reaching a stable size, as seen in Fig. 14. After the first two coating cycles, subsequent deposition yielded no significant changes in agglomerate size distribution. Moreover, the uncoated particles exhibited a broader peak in comparison to those coated with one or two cycles, indicating the formation of a significant quantity of agglomerates smaller than 20 µm (note in Fig. 2 that a considerable amount of small primary particles are present in the powder; clustering of these particles can result in agglomerates of less than 20 µm). The relatively sharp peak observed in particles coated with two cycles suggests a reduction these smaller agglomerates, although we were not able to quantify the extent of their suppression. Furthermore, the emergence of a new peak at approximately 10 µm aligns with the second peak of the bimodal distribution of the primary particles, providing further evidence of successful de-agglomeration of both large and small particle clusters.

The number-based d_{50} and d_{90} of the coated particles, as measured after 30 min in water, when the agglomerate sizes of all samples have stabilized, are presented in Fig. 15. The d_{50} remains nearly unchanged between samples due to its correspondence to the larger primary particles found in the powder, as observed in Fig. 2, potentially including some agglomerates formed by the clustering of smaller particles. The diameter of the largest clusters found in the samples, d_{90}, decreases during the first two coating cycles and remains stable after subsequent deposition. Note that in Fig. 5 we showed additional Si–OH groups to keep forming after the first coating cycle, and Fig. 7 showed full surface coverage after the first coating cycle. These results, combined with the FBRM data imply that surface coverage is the dominant parameter to reduce the agglomerate formation of the polymer micro spheres. We conclude that no additional benefit is gained from increasing the coating thickness and additional functional Si–OH groups once full surface coverage has been achieved. It should be noted that agglomeration occurring during the coating process can hinder the complete surface coverage of individual particles in a single cycle, leaving certain regions of particle contact uncoated. During prolonged fluidization agglomerates can break and reform in a dynamic equilibrium, exposing uncoated areas and facilitating the complete coating of all particles over time. The prior discussion of ESEM images taken of coated particles already touched on the presence of this agglomeration. It is anticipated that these agglomerates are stable under normal handling conditions, clarifying why this effect cannot be seen when employing the previously discussed characterization techniques. However, fully submerging the particles in water is anticipated to cause their disintegration, thereby exposing the uncoated regions, affecting the agglomeration behavior.

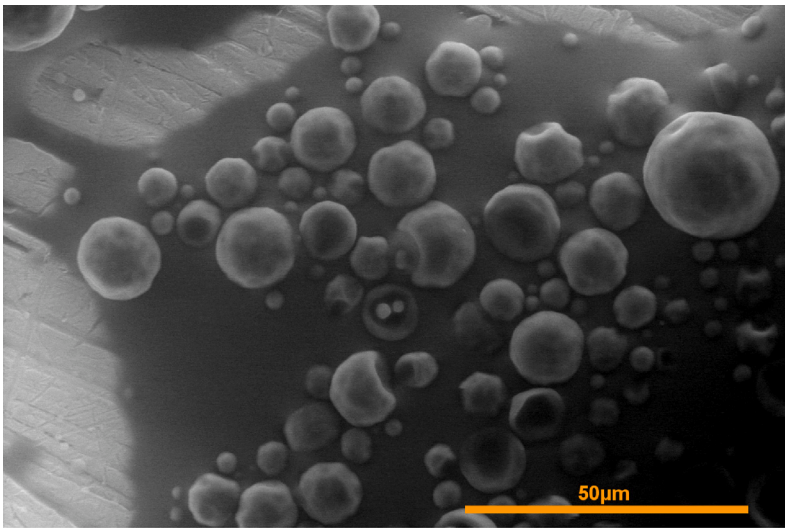

Fig. 8. ESEM image of uncoated powder in the presence of moisture showing limited water-sample affinity.

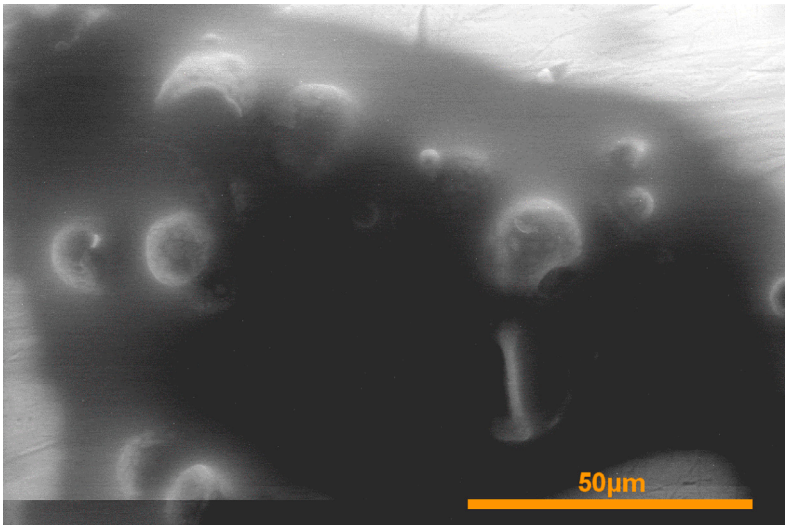

Fig. 9. ESEM image of powder, coated with 1 cycle of SiO_2, in the presence of moisture.

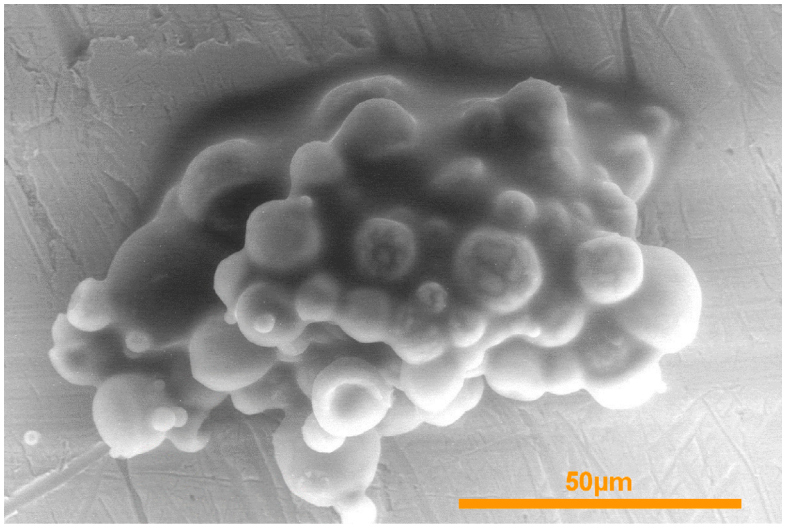

Fig. 10. ESEM image of powder, coated with 5 cycles of SiO_2, in the presence of moisture.

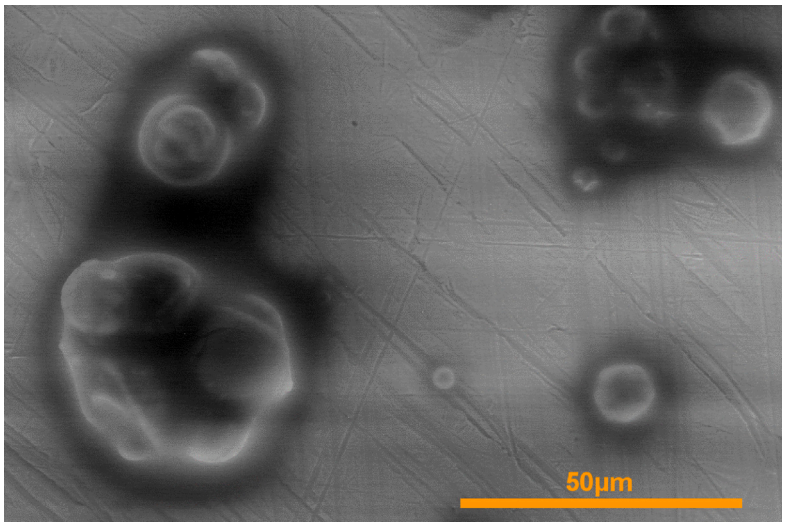

Fig. 11. ESEM image of powder, coated with 10 cycles of SiO_2, in the presence of moisture.

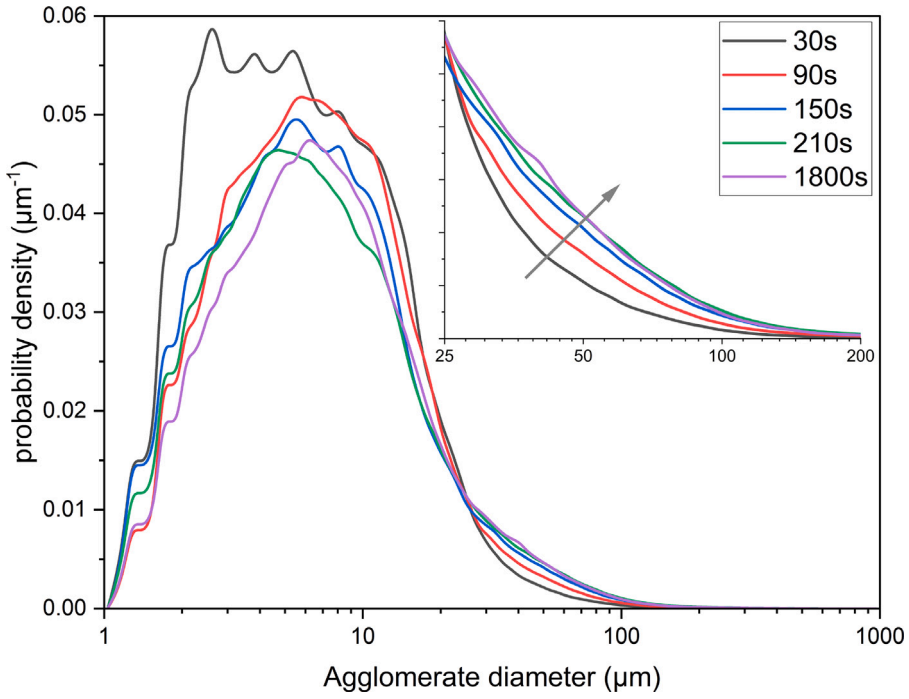

Fig. 12. Number-based agglomerate size distribution development over time of uncoated polymer microspheres in water, measured by FBRM.

This explains the additional decrease in d_{90} observed in Fig. 15 with the application of the second deposition cycle, as it promotes complete coating of all particles.

To substantiate this claim, SEM images of coated particles are provided in Fig. 16 (additional images are provided in the supplementary materials). Particle clusters were intentionally broken up before imaging to reveal uncoated areas resulting from agglomeration. Considering samples, coated with only a single cycle of SiO_2, many non-fully coated particles could be observed, as demonstrated in Fig. 16a. The gaps being circular, implies that the coating was indeed blocked by the presence of particles, attached to the surface by van der Waals forces. Significant gaps were not observed in samples that were subjected to multiple coating cycles. Furthermore, all images in Fig. 16 display a non-uniform coating thickness, which is expected to result from the CVD component within our system.

Additionally, in Fig. 17, we present the findings from the WCA measurements, as well as the measured time for the porous tablet to absorb the entire droplet. The results indicate that the affinity towards water increases after the initial coating cycles, with limited benefits from subsequent deposition. The tested particles were compressed into a tablet prior to experimentation, therefore their mobility was limited. This explains why the effects of exposure of uncoated areas upon the presence of water, as seen during the FBRM experiments, was not observed here. It is important here to note that the preparation of the samples introduces cracks in the coating due to the application of mechanical stress on the particles to pelletize them. This exposes the substrate underneath and alters the surface roughness of the sample, thus contributing to some of the variability in the data. Additionally, we wish to emphasize that the WCA and absorption time measured on pelletized powder substrates should be treated with care since the results might not always be representative of individual particle behavior. These results, however, do confirm the trend observed in the other discussed outcomes, where additional deposition, after achieving full

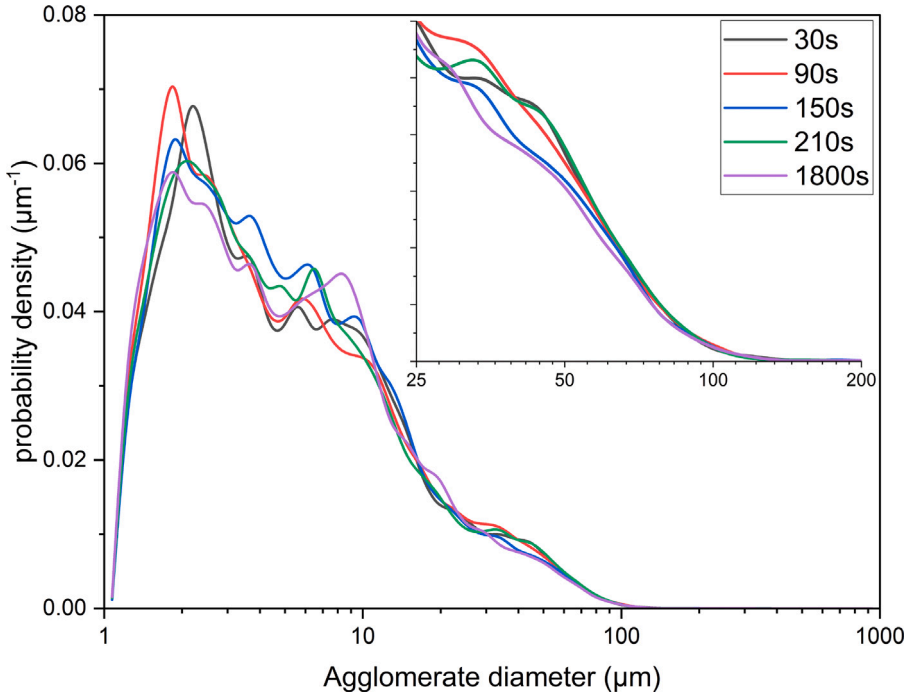

Fig. 13. Number-based agglomerate size distribution development over time of polymer microspheres coated with 1 cycle of SiO_2 in water, measured by FBRM.

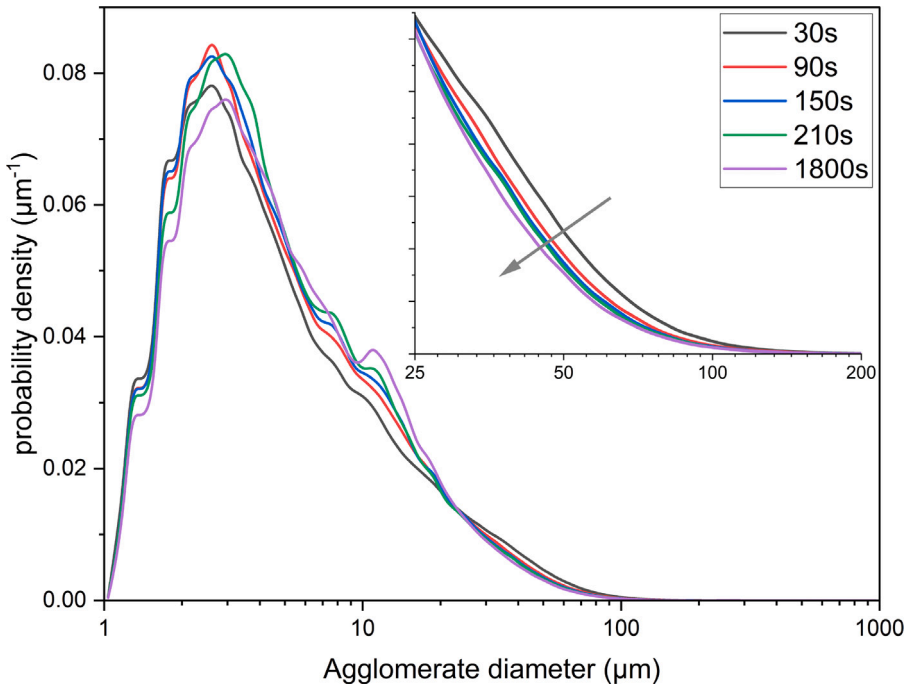

Fig. 14. Number-based agglomerate size distribution development over time of polymer microspheres coated with 2 cycles of SiO_2 in water, measured by FBRM.

surface coverage, has no significant impact on the substrate's affinity towards water.

4. Conclusion

In this investigation, we assessed the impact of a SiO_2 coating, deposited at low temperature in a fluidized bed ALD setup, on the wetting properties of polymer microspheres. Our objective was to introduce hydrophilic Si–OH groups to the particle surface. Their presence was confirmed by FTIR-ATR analysis of the coated substrate. Combined FTIR-ATR, XPS, LEIS and SEM results indicated that a film of SiO_2, covering the entire particle surface, was deposited within the first two coating cycles, with additional cycles thickening this film. Furthermore, insights from applying these techniques demonstrated that the selected conditions under which our system was operated resulted in non-ideal ALD behavior (i.e. pulsed CVD). This lead to the deposition of a film with a considerable thickness (> 4 nm) within the first coating cycle due to the presence of a large CVD component. ESEM imaging demonstrated that the coated agglomerates had a higher tendency to absorb water compared to the uncoated particles. Additional insight

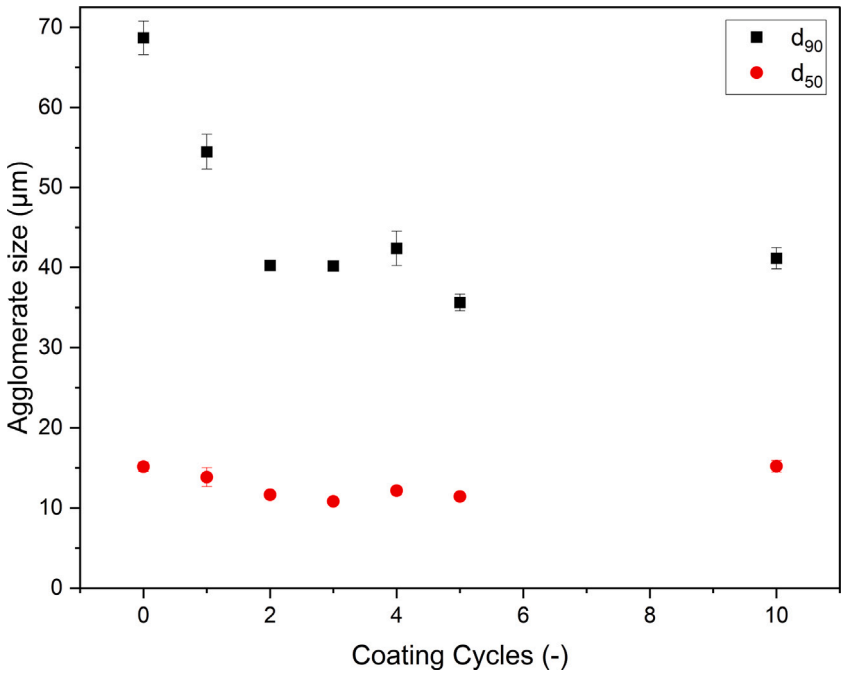

Fig. 15. Agglomerate sizes of pristine and coated powder in water, as measured after 30 min by FBRM (number-based).

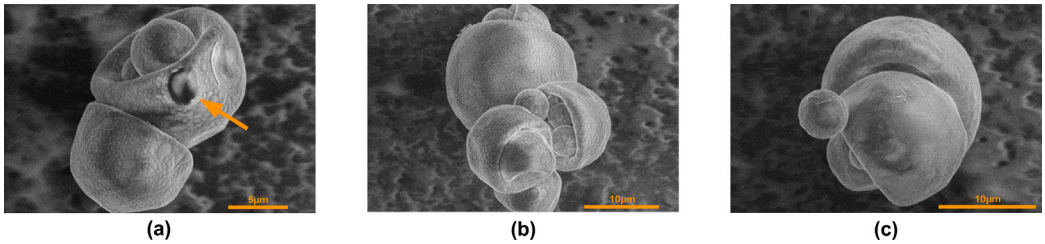

Fig. 16. SEM images of Expancel® powder, coated with **(a)** 1 cycles, **(b)** 2 cycles and **(c)** 10 cycles of SiO_2, the arrow in **(a)** indicates the position of an uncoated spot.

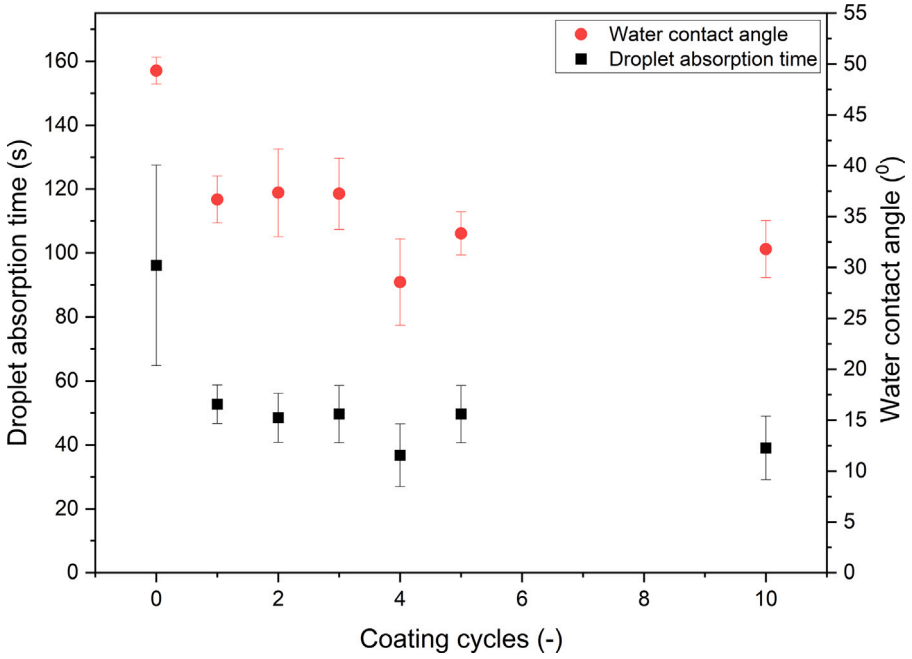

Fig. 17. Water contact angles and absorption time of uncoated and coated sample.

from FBRM data indicated that a second coating cycle provided benefits in reducing agglomerate sizes when brought in contact with water. We anticipate this to be caused by uncoated regions which were subjected to particle–particle contact during the first coating cycle. These regions are revealed upon disintegration of the agglomerates in the presence of water. The uncoated areas can be filled in by consecutive coating cycles, however. More than two coating cycles did not lead to any significant gains in affinity with water, indicating the majority of gaps to have been coated by then. This hypothesis is supported by SEM images of coated samples. Our findings indicate that surface coverage is the key factor in enhancing the stability of a particle–water dispersion by depositing a hydrophilic nanocoating.

CRediT authorship contribution statement

Rens Kamphorst: Conceptualization, Methodology, Validation, Formal analysis, Investigation, Data curation, Writing – original draft, Visualization, Project administration. **Pratyush Wanjari:** Formal analysis, Investigation, Writing – review & editing. **Saeed Saedy:** Conceptualizaton, Formal analysis, Investigation, Writing – review & editing. **Julia F.K. van Dam:** Formal analysis, Investigation. **Arjan Thijssen:** Investigation. **Philipp Brüner:** Investigation. **Thomas Grehl:** Investigation. **Gabrie M.H. Meesters:** Writing – Review & editing, Funding acquisition. **J. Ruud van Ommen:** Writing – Review & editing, Funding acquisition.

Declaration of competing interest

The authors declare that they have no known competing financial interests or personal relationships that could have appeared to influence the work reported in this paper.

Data availability

No data was used for the research described in the article.

Acknowledgments

We want to thank Peter Piechulla for proofreading the manuscript.

This work is part of the Advanced Research Center for Chemical Building Blocks, ARC-CBBC, which is co-founded and co-financed by the Dutch Research Council (NWO) and the Netherlands Ministry of Economic Affairs and Climate Policy.

Appendix A. Supplementary data

Supplementary material related to this article can be found online at https://doi.org/10.1016/j.surfin.2024.103852.

References

[1] N. Garti, I. Yuli-Amar, 6 - Micro- and nano-emulsions for delivery of functional food ingredients, in: N. Garti (Ed.), Delivery and Controlled Release of Bioactives in Foods and Nutraceuticals, in: Woodhead Publishing Series in Food Science, Technology and Nutrition, Woodhead Publishing, 2008, pp. 149–183, http://dx.doi.org/10.1533/9781845694210.2.149.

[2] A. Sullo, I.T. Norton, Food colloids and emulsions, in: B. Caballero, P.M. Finglas, F. Toldrá (Eds.), Encyclopedia of Food and Health, Academic Press, Oxford, 2016, pp. 7–15, http://dx.doi.org/10.1016/B978-0-12-384947-2.00186-0.

[3] N. Singh, A. Joshi, A.P. Toor, G. Verma, Chapter 27 - drug delivery: Advancements and challenges, in: E. Andronescu, A.M. Grumezescu (Eds.), Nanostructures for Drug Delivery, in: Micro and Nano Technologies, Elsevier, 2017, pp. 865–886, http://dx.doi.org/10.1016/B978-0-323-46143-6.00027-0.

[4] M. Agrawal, S. Gupta, M. Stamm, Recent developments in fabrication and applications of colloid based composite particles, J. Mater. Chem. 21 (2011) 615–627, http://dx.doi.org/10.1039/C0JM02631J.

[5] T.F. Tadros, Colloids in Paints, John Wiley and Sons, Ltd, 2010, pp. 1–9, http://dx.doi.org/10.1002/9783527631179.ch1.

[6] H.J. Butt, M. Kappl, Surface and Interfacial Forces, second ed., WILEY-VCH, 2010.

[7] J. Schubert, M. Chanana, Coating matters: Review on colloidal stability of nanoparticles with biocompatible coatings in biological media, living cells and organisms, Curr. Med. Chem. 25 (2018) http://dx.doi.org/10.2174/0929867325666180601101859.

[8] H. Van Bui, F. Grillo, J.R. van Ommen, Atomic and molecular layer deposition: Off the beaten track, Chem. Commun. 53 (2017) 45–71, http://dx.doi.org/10.1039/C6CC05568K.

[9] R.W. Johnson, A. Hultqvist, S.F. Bent, A brief review of atomic layer deposition: From fundamentals to applications, Mater. Today 17 (5) (2014) 236–246, http://dx.doi.org/10.1016/j.mattod.2014.04.026.

[10] L. Sun, G. Yuan, L. Gao, J. Yang, M. Chhowalla, K. Heydari Gharahcheshmeh, Y. Choi, B. Hong, Z. Liu, Chemical vapour deposition, 1 (2021) 5. http://dx.doi.org/10.1038/s43586-020-00005-y.

[11] D. Muñoz-Rojas, V.H. Nguyen, C. Masse de la Huerta, S. Aghazadehchors, C. Jiménez, D. Bellet, Spatial Atomic Layer Deposition (SALD), an emerging tool for energy materials. Application to new-generation photovoltaic devices and transparent conductive materials, C. R. Phys. 18 (7) (2017) 391–400, http://dx.doi.org/10.1016/j.crhy.2017.09.004.

[12] J.R. van Ommen, A. Goulas, Atomic layer deposition on particulate materials, Mater. Today Chem. 14 (2019) 100183, http://dx.doi.org/10.1016/j.mtchem.2019.08.002.

[13] J. Guo, D. Benz, T.-T. Doan Nguyen, P.-H. Nguyen, T.-L. Thi Le, H.-H. Nguyen, D. La Zara, B. Liang, H.T.B. Hintzen, J.R. van Ommen, H. Van Bui, Tuning the photocatalytic activity of TiO2 nanoparticles by ultrathin SiO2 films grown by low-temperature atmospheric pressure atomic layer deposition, Appl. Surf. Sci. 530 (2020) 147244, http://dx.doi.org/10.1016/j.apsusc.2020.147244.

[14] R. Kamphorst, K. Wu, S. Salameh, G.M.H. Meesters, J.R. van Ommen, On the fluidization of cohesive powders: Differences and similarities between micro- and nano-sized particle gas–solid fluidization, Can. J. Chem. Eng. 101 (1) (2023) 227–243, http://dx.doi.org/10.1002/cjce.24615.

[15] D. Geldart, N. Harnby, A.C. Wong, Fluidization of cohesive powders, Powder Technol. 37 (1) (1984) 25–37, http://dx.doi.org/10.1016/0032-5910(84)80003-0.

[16] R. Kamphorst, P.C. van der Sande, K. Wu, E.C. Wagner, M.K. David, G.M.H. Meesters, J.R. van Ommen, The mechanism behind vibration assisted fluidization of cohesive micro-silica, KONA Powder Part. J. advpub (2023) 2024007, http://dx.doi.org/10.14356/kona.2024007.

[17] H. Azizpour, M. Talebi, F.D. Tichelaar, R. Sotudeh-Gharebagh, J. Guo, J.R. van Ommen, N. Mostoufi, Effective coating of titania nanoparticles with alumina via atomic layer deposition, Appl. Surf. Sci. 426 (2017) 480–496, http://dx.doi.org/10.1016/j.apsusc.2017.07.168.

[18] S. Ali, E. AL-Ghurabi, A. Ajbar, Y. Mohammed, M. Boumaza, M. Asif, Effect of frequency on pulsed fluidized beds of ultrafine powders, J. Nanomater. 2016 (2016) 1–12, http://dx.doi.org/10.1155/2016/4592501.

[19] S. Ebnesajjad, Chapter 4 - surface and material characterization techniques, in: S. Ebnesajjad (Ed.), Surface Treatment of Materials for Adhesive Bonding (Second Edition), second ed., William Andrew Publishing, Oxford, 2014, pp. 39–75, http://dx.doi.org/10.1016/B978-0-323-26435-8.00004-6.

[20] P. Launer, B. Arkles, Infrared Analysis of Organosilicon Compounds, 2013, pp. 175–178.

[21] M.F. Omar, K. Ismail, I. Sumpono, E. Albert Alim, M. Nawi, M. Mukri, Z. Othaman, S. Sakrani, FTIR spectroscopy characterization of Si-C bonding in SiC thin film prepared at room temperature by conventional 13.56 MHz RF PECVD, Malays. J. Fundam. Appl. Sci. 8 (2012) http://dx.doi.org/10.11113/mjfas.v8n4.156.

[22] F. Yan, J. Jianguo, X. Chen, S. Tian, K. Li, Synthesis and characterization of silica nanoparticles preparing by low-temperature vapor-phase hydrolysis of SiCl4, Ind. Eng. Chem. Res. 53 (2014) 11884–11890, http://dx.doi.org/10.1021/ie501759w.

[23] P. Pinto, L.C. Mendes, M. Dias, C. Azuma, Synthesis of acrylic-modified sol–gel silica, Colloid Polym. Sci. 284 (2006) 529–535, http://dx.doi.org/10.1007/s00396-005-1424-0.

[24] S. Salameh, M.A. van der Veen, M. Kappl, J.R. van Ommen, Contact forces between single metal oxide nanoparticles in gas-phase applications and processes, Langmuir 33 (10) (2017) 2477–2484, http://dx.doi.org/10.1021/acs.langmuir.6b02982.